

## Graphene Anchored with Nanocrystal Fe<sub>2</sub>O<sub>3</sub> with Improved Electrochemical Li-Storage Properties

Shuang-Yu Liu, Jian Xie, Qin Pan, Chun-Yang Wu, Gao-Shao Cao, Tie-Jun Zhu and, Xin-Bing Zhao\*

Department of Materials Science and Engineering, Zhejiang University, Hangzhou 310027, China

\*E-mail: [zhaorb@zju.edu.cn](mailto:zhaorb@zju.edu.cn)

Received: 31 October 2011 / Accepted: 10 December 2011 / Published: 1 January 2012

---

Graphene anchored with nanocrystal Fe<sub>2</sub>O<sub>3</sub> was synthesized by a two-step solvothermal route. The nanocomposite was characterized by X-ray diffraction (XRD), Raman spectra, X-ray photoelectron spectroscopy (XPS), thermogravimetric analysis (TGA), scanning electron spectroscopy (SEM) and transmission electron microscopy (TEM). It was found that the Fe<sub>2</sub>O<sub>3</sub> nano-particles were formed and homogeneously anchored on graphene sheets. The electrochemical properties of the nanocomposite were investigated by galvanostatic cycling. The results showed that the Fe<sub>2</sub>O<sub>3</sub>/graphene nanocomposite exhibits obviously improved electrochemical properties compared to bare Fe<sub>2</sub>O<sub>3</sub> because of the buffering, confining and conducting effects of the introduced graphene.

---

**Keywords:** Fe<sub>2</sub>O<sub>3</sub>, graphene, nanocomposite, electrochemical properties, anode

### 1. INTRODUCTION

In the early 1980s, some transition metal oxides, such as CuO [1], Fe<sub>2</sub>O<sub>3</sub> [2], and CoO [3] have already been used as cathode in primary batteries. In recent years, these oxides have received a renewed interest since they showed reversible cycling as anodes for Li-ion batteries [4–7]. Among these oxides, Fe<sub>2</sub>O<sub>3</sub> is an attractive anode material for lithium ion batteries due to the high theoretical capacity (1005mAh g<sup>-1</sup>), high abundance of Fe, low cost and low environmental impact [8–10]. However, Fe<sub>2</sub>O<sub>3</sub> generally shows a rapid capacity fade because of the large volume changes and agglomerations during the conversion reactions. Great effort has been made to improve the electrochemical properties of Fe<sub>2</sub>O<sub>3</sub>. A stable cycling could be obtained for Fe<sub>2</sub>O<sub>3</sub> by using nanostructured [11, 12], porous [13] and thin-film materials [14] with relieved volume changes.

Dispersing the particles on conducting carbon materials has been proved to be a useful strategy to improve cycling stability of the transition metal oxides due to the effective buffering and conducting effects of carbon materials. In addition, carbon materials also contribute to the overall capacity for the

composite. Various forms of carbon, such as amorphous carbon [15], carbon fibers [16], and carbon nanotubes [17] have been suggested as the ideal matrices to disperse  $\text{Fe}_2\text{O}_3$ . Recently, great importance has been attached to another form of carbon, graphene, since reported by Novoselov et al. in 2004 [18]. The intensive researches on tin oxides [19-22], cobalt oxides [23–29], and copper oxides [30, 31] have shown that the cycling stability of these oxides could be greatly improved by loading them onto the graphene.

Graphene, a flat monolayer of  $\text{sp}^2$ -bonded carbon atoms, is considered as an ideal matrix to disperse nanoparticles due to its advantages such as large specific surface area [32], high electronic conductivity [33], and high mechanical strength [34]. These merits make graphene or graphene-based materials very promising for use as anode materials for Li-ion batteries. In this work, we will investigate the effect of graphene on the electrochemical performance of  $\text{Fe}_2\text{O}_3$ . The  $\text{Fe}_2\text{O}_3/\text{graphene}$  ( $\text{Fe}_2\text{O}_3/\text{G}$ ) nanocomposite was prepared by a two-step solvothermal route. The results showed that the nanocomposite exhibits an obviously improved cycling stability compared with bare  $\text{Fe}_2\text{O}_3$ .

## 2. EXPERIMENTAL SECTION

### 2.1 Synthesis of $\text{Fe}_2\text{O}_3/\text{graphene}$ nanocomposite

Graphite oxide (GO, 20 mg), synthesized by a modified Hummer's method [35], was ultrasonically dispersed in a *N,N*-dimethylformamide (DMF)/ $\text{H}_2\text{O}$  (10:1 in volume) mixed solvent for 1 h to get graphene oxide followed by adding of 1 mmol  $\text{FeSO}_4 \cdot 7\text{H}_2\text{O}$ . The above dispersion was then heated at 80 °C for 3 h. Afterwards, the mixture was sealed into a Teflon-lined stainless steel autoclave and maintained at 180 °C for 20 h. After it was cooled down to the room temperature, the resulting product was separated by centrifugation, washed with deionized water and ethanol for several times, and dried at 40 °C under vacuum overnight. For comparison, bare  $\text{Fe}_2\text{O}_3$  was prepared using the similar procedure without adding GO.

### 2.2 Materials Characterization

X-ray diffraction (XRD) patterns of the products were collected on a Rigaku D/Max-2550pc powder diffractometer equipped with  $\text{Cu K}_\alpha$  radiation ( $\lambda = 1.541 \text{ \AA}$ ). X-ray photoelectron spectroscopy (XPS) analysis was performed on a KRATOS AXIS ULTRA-DLD spectrometer with a monochromatic  $\text{Al K}_\alpha$  radiation ( $h\nu = 1486.6 \text{ eV}$ ). The microstructures were observed by field emission scanning electron microscopy (FE-SEM) on a FEI-sirion microscope and transmission electron microscopy (TEM) on a JEM 2100F microscope. Raman spectra were recorded on a Jobin-Yvon Labor Raman HR-800 using 514.5 nm Ar-ion laser. Thermogravimetric analysis (TGA) was performed on a DSCQ1000 instrument from 80 to 800 °C at a heating rate of 10 °C  $\text{min}^{-1}$  in air.

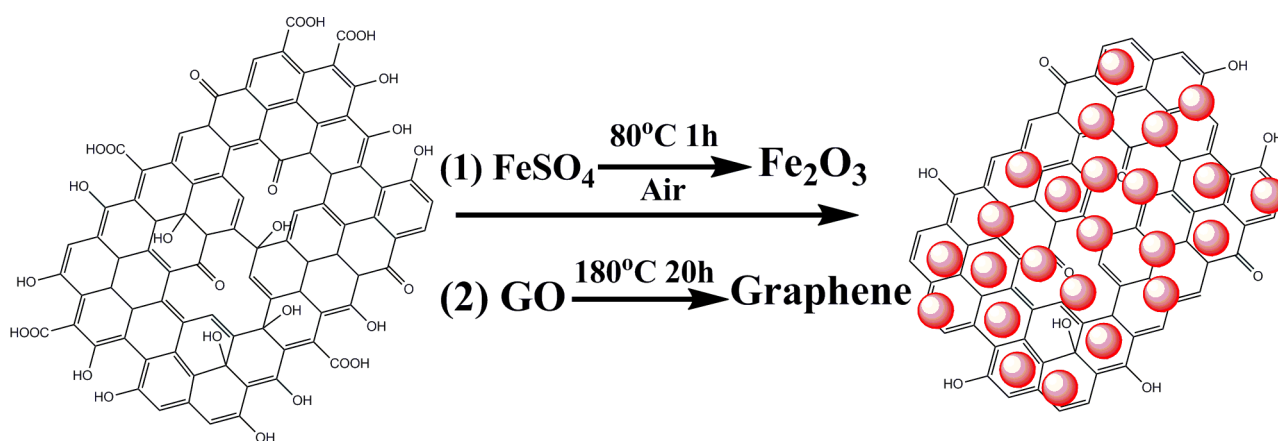
### 2.3 Electrochemical measurements

The electrochemical properties of the products ( $\text{Fe}_2\text{O}_3/\text{G}$ ,  $\text{Fe}_2\text{O}_3$ ) were evaluated using CR2025-type coin cells. The electrode slurry was prepared by mixing the active material, acetylene black and

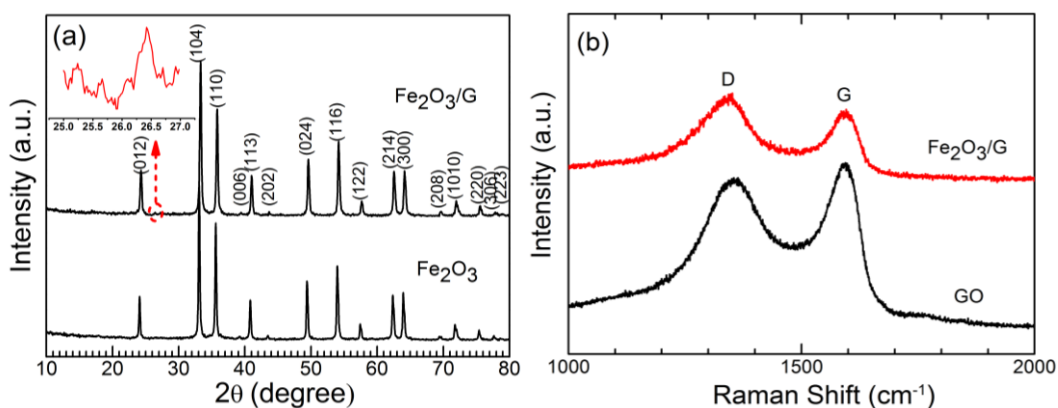
polyvinylidene fluoride in a weight ratio of 75:15:10 in N-methyl pyrrolidone (NMP) with stirring for 2 h. The working electrodes were made by coating the slurry onto Ni foam current collectors and dried at 100 °C under vacuum overnight. The working electrodes were assembled into half cells in an Ar-filled glove box using Li foil as the counter electrode and polypropylene microporous sheet (Celgard 2300) as the separator. The electrolyte was 1 M LiPF<sub>6</sub> dissolved in ethylene carbonate (EC)/dimethyl carbonate (DMC) (1:1, in volume). The cells were galvanostatically charged and discharged between 0.005 and 3 V (vs. Li/Li<sup>+</sup>) on a Neware BTS-5V10mA battery cycler (Shenzhen, China). Cyclic voltammetry (CV) measurements were conducted on an Arbin BT2000 system in the voltage range 0.005–3.0 V (vs. Li/Li<sup>+</sup>) at 0.1 mV s<sup>-1</sup>. Electrochemical impedance spectroscopy (EIS) measurements were performed on a CHI660C electrochemistry workstation by applying an ac voltage of 5 mV amplitude in the frequency range from 10 mHz to 100 kHz at de-lithiated states. All of the electrochemical measurements were carried out at room temperature.

### 3. RESULTS and DISCUSSION

The two-step solvothermal route for Fe<sub>2</sub>O<sub>3</sub>/G synthesis is schematically illustrated in Fig. 1.



**Figure 1.** Schematic illustration of the synthetic route of Fe<sub>2</sub>O<sub>3</sub>/G.



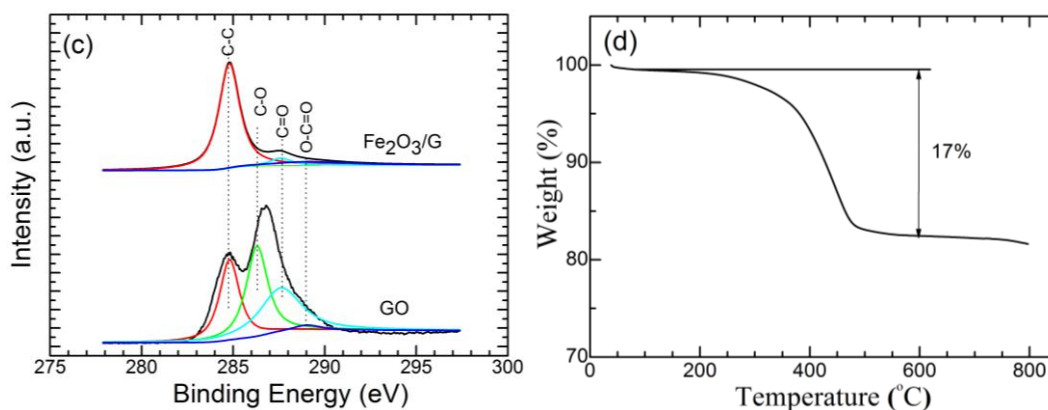
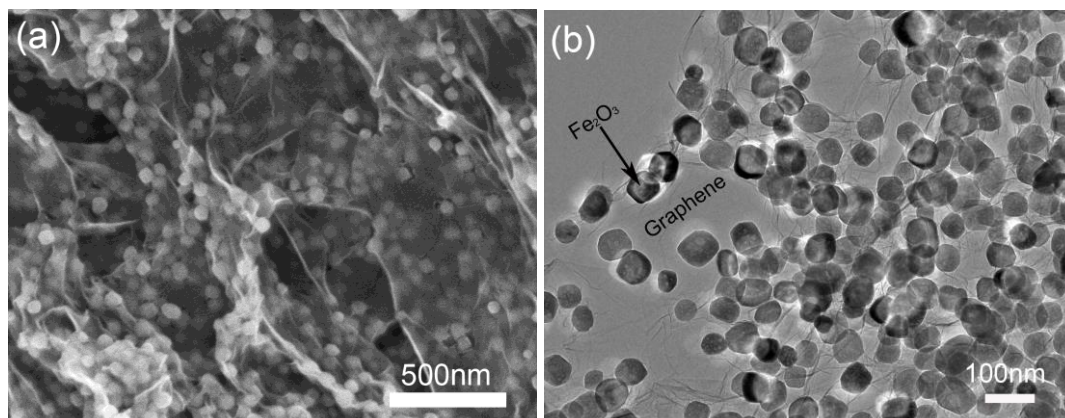


**Figure 2.** (a) XRD patterns of  $\text{Fe}_2\text{O}_3/\text{G}$  and bare  $\text{Fe}_2\text{O}_3$ , (b) Raman spectra of  $\text{Fe}_2\text{O}_3/\text{G}$  and GO, (c) C1s XPS of  $\text{Fe}_2\text{O}_3/\text{G}$  and GO, and (d) thermogravimetric analysis of  $\text{Fe}_2\text{O}_3/\text{G}$ .

In the first step, The  $\text{Fe}^{2+}$  was undergoes oxidation and hydrolysis in DMF/ $\text{H}_2\text{O}$  to form  $\text{Fe}_2\text{O}_3$  nanoparticles which are uniformly anchored on the graphene oxide sheets. In the second step, the graphene oxide was reduced to graphene to form the final product  $\text{Fe}_2\text{O}_3/\text{G}$ .

Fig. 2(a) shows the XRD patterns of  $\text{Fe}_2\text{O}_3/\text{G}$  and  $\text{Fe}_2\text{O}_3$ . The dominant diffraction peaks can be assigned to  $\text{Fe}_2\text{O}_3$  for both  $\text{Fe}_2\text{O}_3/\text{G}$  and  $\text{Fe}_2\text{O}_3$  (JCPDS No. 33-0664). A hump appears in the range of  $26\text{-}27^\circ$  ( $2\theta$ ), which originates from graphene as seen in the inset of Fig. 2(a). The small diffraction peak of graphene indicates that the graphene sheets are sufficiently exfoliated by the attached  $\text{Fe}_2\text{O}_3$  nanoparticles. Fig. 2(b) gives the Raman spectra of GO and  $\text{Fe}_2\text{O}_3/\text{G}$ . Both the samples present two bands at  $1350$  and  $1580\text{ cm}^{-1}$ , which correspond to the disordered (D) band and graphitic (G) band of carbon materials [36]. Compared with GO,  $\text{Fe}_2\text{O}_3/\text{G}$  exhibits an increased D/G intensity ratio, indicating the conversion from GO to graphene [37].

The conversion of GO into graphene is further proved by XPS analysis as shown in Fig. 2(c). The XPS spectra can be fitted into four peaks, corresponding to carbon atoms in four functional groups:  $\text{sp}^2$  carbon (C-C,  $284.8\text{ eV}$ ), carbon in C-O bonds ( $286.3\text{ eV}$ ), carbonyl carbon (C=O,  $287.6\text{ eV}$ ) and carboxylate carbon (O-C=O,  $290.0\text{ eV}$ ) [37].



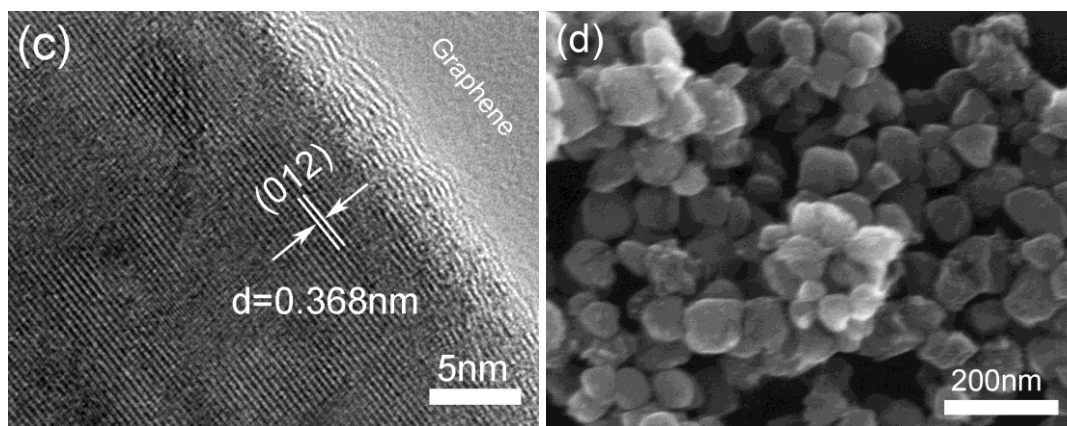


**Figure 3.** (a) SEM, (b) TEM, (c) HRTEM images of  $\text{Fe}_2\text{O}_3/\text{G}$ , and (d) SEM images of bare  $\text{Fe}_2\text{O}_3$ .

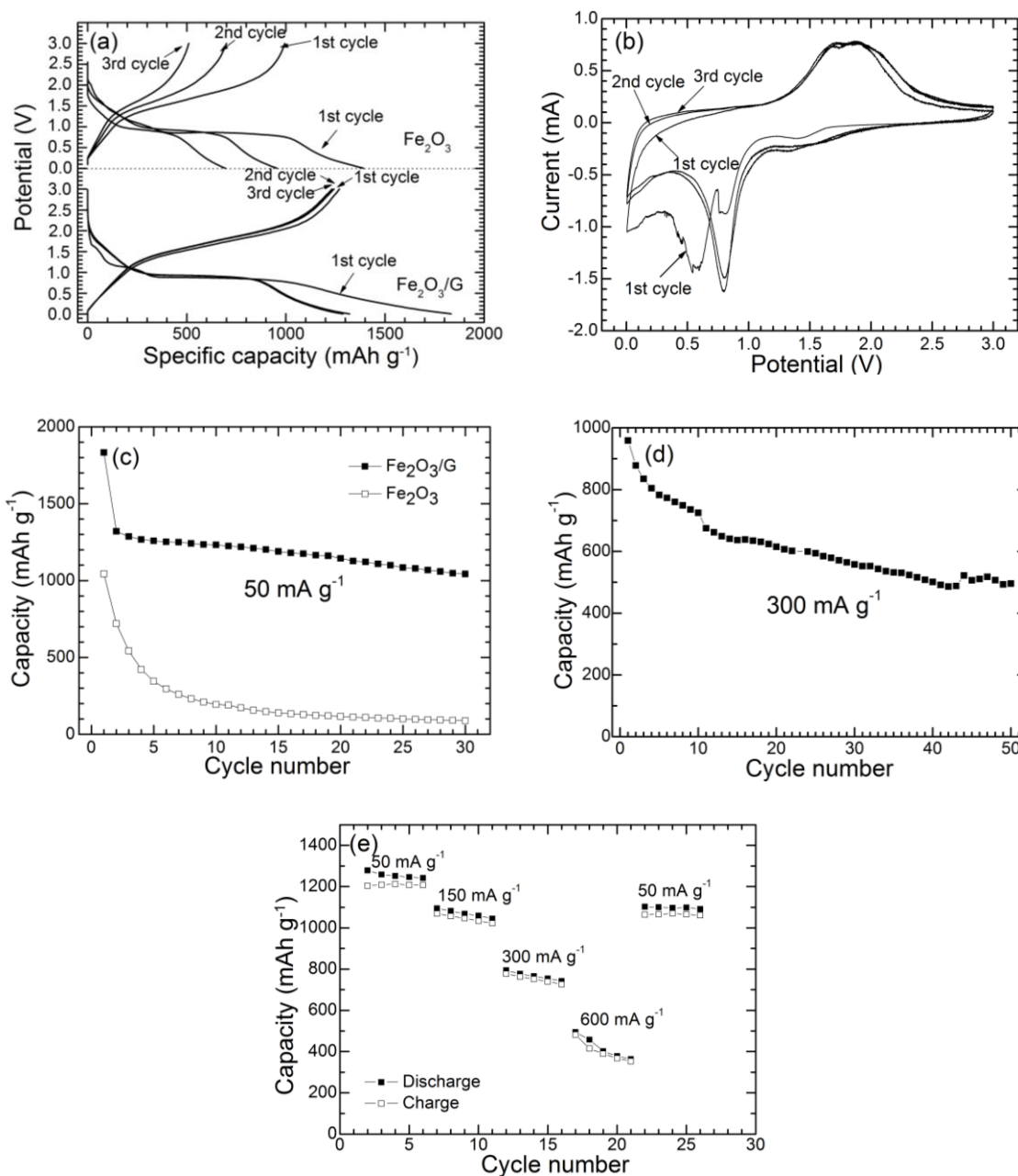
After the solvothermal reaction, the peak intensity of carbons in C-O, C=O and O-C=O shows a considerable decrease, confirming that a sufficient reduction of graphene oxide to graphene has occurred. The weight ratio of  $\text{Fe}_2\text{O}_3$  and graphene was determined by TGA in air as shown in Fig. 2(d). The graphene content is estimated to 17% according to TGA.

Fig. 3(a) shows the SEM images of  $\text{Fe}_2\text{O}_3/\text{G}$  synthesized by the solvothermal route at 180 °C. Through the transparent graphene, it is clear that the  $\text{Fe}_2\text{O}_3$  nanoparticles are uniformly confined in between the graphene sheets. The nanoparticles show a firm attachment with graphene even though undergone vigorous sonication, implying a strong interaction between graphene and  $\text{Fe}_2\text{O}_3$ . The TEM images in Fig. 3(b) clearly show that the  $\text{Fe}_2\text{O}_3$  particles with a size of 50–80 nm are homogeneously dispersed by graphene. Fig. 3(c) displays the HRTEM images of an individual  $\text{Fe}_2\text{O}_3$  particle on graphene. The fringe spacing is measured to be 0.368 nm, corresponding to the interplanar spacing of (012) plane of  $\text{Fe}_2\text{O}_3$ . Without the confinement by graphene, the  $\text{Fe}_2\text{O}_3$  nanoparticles tend to aggregate as shown in Fig. 3(d).

To study the Li-ion storage properties of  $\text{Fe}_2\text{O}_3/\text{G}$  and bare  $\text{Fe}_2\text{O}_3$ , a series of electrochemical measurements were carried out. Fig. 4(a) shows the charge-discharge curves of bare  $\text{Fe}_2\text{O}_3$  and  $\text{Fe}_2\text{O}_3/\text{G}$  for the first three cycles at  $50\text{mA g}^{-1}$ . The first charge (Li-extraction) and discharge (Li-insertion) of  $\text{Fe}_2\text{O}_3/\text{G}$  are 1270 and 1833 mAh  $\text{g}^{-1}$ , respectively. The  $\text{Fe}_2\text{O}_3/\text{G}$  electrode exhibits a highly reversible cycling evidenced from the almost overlapped charge or discharge curves except for the first cycle. The high reversibility of  $\text{Fe}_2\text{O}_3/\text{G}$  could be ascribed to the homogeneous dispersion of the  $\text{Fe}_2\text{O}_3$  nanoparticles by the highly conductive graphene [38]. In contrast, a large first irreversible capacity and a rapid capacity fade are observed for bare  $\text{Fe}_2\text{O}_3$ . Fig. 4(b) shows the CV plots of  $\text{Fe}_2\text{O}_3/\text{G}$  at a scan rate of  $0.1\text{ mV s}^{-1}$ . The oxidation and reduction peaks are fixed at around 1.9 V and 0.8 V, respectively, after the first cycle, also indicating the reversible cycling of the electrode.

Fig. 4(c) compares the cycling stability between bare  $\text{Fe}_2\text{O}_3$  and  $\text{Fe}_2\text{O}_3/\text{G}$  at  $50\text{mA g}^{-1}$ . Obviously,  $\text{Fe}_2\text{O}_3/\text{G}$  shows an improved cycling stability than bare  $\text{Fe}_2\text{O}_3$ . After 30 cycles,  $\text{Fe}_2\text{O}_3/\text{G}$  still maintains a discharge capacity of  $1043\text{ mAh g}^{-1}$ , while for bare  $\text{Fe}_2\text{O}_3$ , its capacity drops rapidly to  $89\text{ mAh g}^{-1}$  after the same cycles. The cycling performance of the  $\text{Fe}_2\text{O}_3/\text{G}$  electrode at  $300\text{ mA g}^{-1}$  was also evaluated as shown in Fig. 4(d). After 50 cycles,  $\text{Fe}_2\text{O}_3/\text{G}$  still retains a capacity of 496 mAh

$\text{g}^{-1}$ . The enhancement in cycling stability could be attributed to the introduction of graphene that acts both as a buffer to accommodate the volume changes and as a separator to prevent the  $\text{Fe}_2\text{O}_3$  nanoparticles from aggregating.



**Figure 4.** Electrochemical properties of the solvothermal products: (a) charge-discharge curves of  $\text{Fe}_2\text{O}_3/\text{G}$  and bare  $\text{Fe}_2\text{O}_3$  at  $50 \text{ mA g}^{-1}$ , (b) CV plots of  $\text{Fe}_2\text{O}_3/\text{G}$  at  $0.1 \text{ mV s}^{-1}$ , (c) comparison of cycling stability between  $\text{Fe}_2\text{O}_3/\text{G}$  and bare  $\text{Fe}_2\text{O}_3$  at  $50 \text{ mA g}^{-1}$ , (d) cycling stability of  $\text{Fe}_2\text{O}_3/\text{G}$  at  $300 \text{ mA g}^{-1}$ , and (e) rate capability of  $\text{Fe}_2\text{O}_3/\text{G}$ .

Fig. 4e shows the rate capability of  $\text{Fe}_2\text{O}_3/\text{G}$ . Note that  $\text{Fe}_2\text{O}_3/\text{G}$  exhibits a good rate capability. After being cycled at high rates, the capacity can be well recovered once the current is shifted to a low

value, indicating a good reversibility for  $\text{Fe}_2\text{O}_3/\text{G}$ . The good rate capability comes mainly from the two factors: first, the highly conductive graphene supplies two-dimensional (2D) conducting channels for the  $\text{Fe}_2\text{O}_3$  nanoparticles; second, the homogeneous dispersion of  $\text{Fe}_2\text{O}_3$  nanoparticles by graphene leads to a good wetting of the active material by the electrolyte and thus facilitates the rapid Li-ion diffusion at the electrode/electrolyte interface. Furthermore, the small-sized  $\text{Fe}_2\text{O}_3$  is also favorable for rapid Li-ion solid phase diffusion when it is effectively confined by graphene.

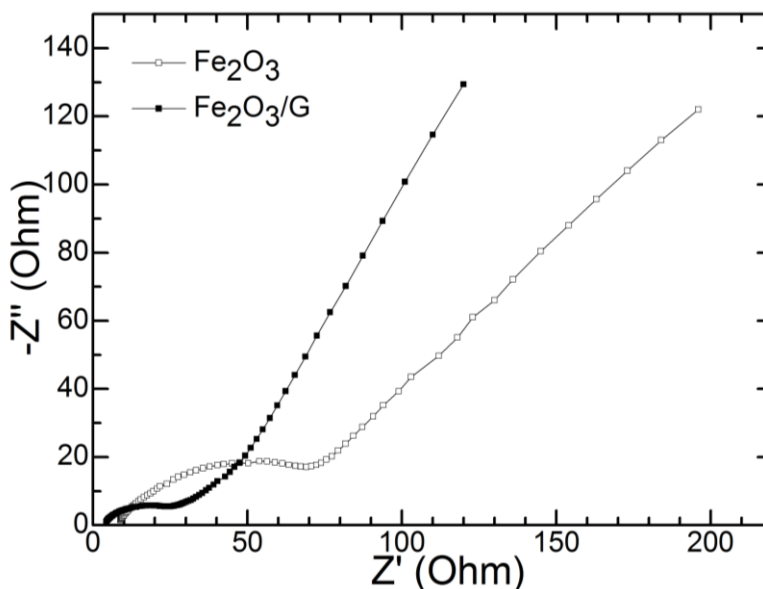


**Figure 5.** Nyquist plots of  $\text{Fe}_2\text{O}_3/\text{G}$  and bare  $\text{Fe}_2\text{O}_3$  electrodes after 10 cycles

EIS measurements were carried out to understand the effect of graphene on the electrochemical behaviors of  $\text{Fe}_2\text{O}_3$ . Fig.5 gives the Nyquist plots of the  $\text{Fe}_2\text{O}_3$  and  $\text{Fe}_2\text{O}_3/\text{G}$  composites after 10 charge-discharge cycles. The plots are composed of two partially overlapped semicircles at high- and medium-frequency ranges and a sloping line at the low frequency range. The high-frequency semicircle corresponds to the solid electrolyte interface (SEI) layer resistance  $R_{\text{SEI}}$ ; the middle-frequency semicircle is related to the charge transfer resistance  $R_{\text{ct}}$ ; the sloping line at the low frequency is associated with the Li-ion solid phase diffusion in the bulk electrode. The  $\text{Fe}_2\text{O}_3/\text{G}$  electrode shows smaller  $R_{\text{SEI}}$  and  $R_{\text{ct}}$  than the bare  $\text{Fe}_2\text{O}_3$  electrode. The better wetting the active material and refrained particles aggregation are responsible for the low  $R_{\text{ct}}$  value for  $\text{Fe}_2\text{O}_3/\text{G}$ . The stabilization of the electrode by confining the active particles between the graphene sheets is considered to account for its low  $R_{\text{SEI}}$  value. A lower  $R_{\text{ct}}$  for  $\text{Fe}_2\text{O}_3/\text{G}$  can explain its good cycling stability and rate capability. In addition, a low  $R_{\text{SEI}}$  value is also beneficial for the reversible cycling of the electrode. As a result, the EIS measurements agree well with the different electrochemical behaviors of  $\text{Fe}_2\text{O}_3$  with and without graphene.

#### 4. CONCLUSIONS

Fe<sub>2</sub>O<sub>3</sub>-graphene nanocomposites have been synthesized by a two-step solution route. The nanoparticles with an average size of 50–80 nm are uniformly anchored on graphene. The nanocomposite shows improved electrochemical properties compared to the bare oxide. The improvement in electrochemical performance is attributed to the flexible graphene that not only buffers the volume changes but also refrains the aggregation of nanoparticles. The introduced graphene also offers a 2D conductive network and increases the wetting of the active material, also contributing to enhanced electrochemical performance.

#### ACKNOWLEDGEMENTS

This work was supported by Zijin Program of Zhejiang University, China, the Fundamental Research Funds for the Central Universities (No. 2010QNA4003), the Ph.D. Programs Foundation of Ministry of Education of China (No. 20100101120024), the Foundation of Education Office of Zhejiang Province (No. Y201016484), the Qianjiang Talents Project of Science Technology Department of Zhejiang Province (2011R10021), and the National Natural Science Foundation of China (No. 51101139).

#### References

1. T. Iijima, Y. Toyoguchi, J. Nishimura, and H. Ogawa, *J. Power Sources* 5 (1980) 99.
2. M. M. Thackeray and J. Coetzer, *Mater. Res. Bull.* 16 (1981) 591.
3. M. M. Thackeray, S. D. Baker, and J. Coetzer, *Mater. Res. Bull.* 1 (1982) 405.
4. P. Poizot, S. Laruelle, S. Grugeon, L. Dupont, and J. M. Tarascon, *Nature* 407 (2000) 496.
5. A. Débart, L. Dupont, P. Poizot, J. B. Leriche, and J. M. Tarascon, *J. Electrochem. Soc.* 148 (2001) A1266.
6. S. Grugeon, S. Laruelle, R. Herrera-Urbina, L. Dupont, P. Poizot, and J. M. Tarascon, *J. Electrochem. Soc.* 148 (2001) A285.
7. F. Badway, I. Plitz, S. Grugeon, S. Laruelle, M. Dollé, A. S. Gozdz, and J. M. Tarascon, *Electrochem. Solid State Lett.* 5 (2002) A115.
8. H. Liu, G. Wang, J. Park, J. Wang, H. Liu, and C. Zhang, *Electrochim. Acta.* 54 (2009) 1733.
9. L. C. Yang, Q. S. Gao, Y. H. Zhang, Y. Tang, and Y. P. Wu, *Electrochem. Commun.* 10 (2008) 118.
10. H. Liu, D. Wexler, and G. Wang, *J. Alloys Compd.* 487 (2009) L24.
11. Y. N. NuLi, R. Zeng, P. Zhang, Z. P. Guo, and H. K. Liu, *J. Power Sources* 184 (2008) 456.
12. J. P. Liu, Y. Y. Li, H. J. Fan, Z. H. Zhu, J. Jiang, R. M. Ding, Y. Y. Hu, and X. T. Huang, *Chem. Mater.* 22 (2010) 212.
13. B. Sun, J. Horvat, H. S. Kim, W. S. Kim, J. Ahn, and G. X. Wang, *J. Phys. Chem. C* 114 (2010) 18753.
14. L. Wang, H. W. Xu, P. C. Chen, D. W. Zhang, C. X. Ding, and C. H. Chen, *J. Power Source* 193 (2009) 846.
15. M. G. B. Sassin, A. N. Mansour, K. A. Pettigrew, D. R. Rolison, and J. W. Long, *ACS Nano* 8 (2010) 4505.
16. M. S. Wu, Y. H. Ou, and Y. P. Lin, *Electrochim. Acta* 55 (2010) 3240.
17. S. L. Chou, J. Z. Wang, Z. X. Chen, H. K. Liu, and S. X. Dou, *Nanotechnology* 22 (2011) 265401.
18. K. S. Novoselov, A. K. Geim, S. V. Morozov, D. Jiang, Y. Zhang, S. V. Dubonos, I. V. Grigorieva, and A. A. Firsov, *Science* 306 (2004) 666.



19. D. H. Wang, R. Kou, D. W. Choi, Z. G. Yang, Z. M. Nie, J. Li, L. V. Saraf, D. H. Hu, J. H. Zhang, G. L. Graff, J. Liu, M. A. Pope, and I. A. Aksay, *ACS Nano* 3 (2010) 1587.
20. S. M. Paek, E. J. Yoo, and I. Honma, *Nano Lett.* 9 (2009) 72.
21. J. Yao, X. P. Shen, B. Wang, H. K. Liu, and G. X. Wang, *Electrochem. Commun.* 11 (2009) 1849.
22. L. S. Zhang, L. Y. Jiang, H. J. Yan, W. D. Wang, W. Wang, W. G. Song, Y. G. Guo, and L. J. Wan, *J. Mater. Chem.* 20 (2010) 5462.
23. S. Q. Chen and Y. Wang, *J. Mater. Chem.* 20 (2010) 9735.
24. Z. S. Wu, W. C. Ren, L. Wen, L. B. Gao, J. P. Zhao, Z. P. Chen, G. M. Zhou, F. Li, and H. M. Cheng, *ACS Nano* 4 (2010) 3187.
25. S. B. Yang, X. L. Feng, S. Ivanovici, and K. Müllen, *Angew. Chem. Int. Ed.* 49 (2010) 8408.
26. H. Kim, D.H. Seo, S.W. Kim, J. Kim, and K. Kang, *Carbon* 49 (2011) 326.
27. B. J. Li, H. Q. Cao, J. Shao, G. Q. Li, M. Z. Qu, and G. Yin, *Inorg. Chem.* 50 (2011) 1628.
28. J. X. Zhu, Y. K. Sharma, Z. Y. Zheng, X. J. Zhang, M. Srinivasan, S. Mhaisalkar, H. Zhang, H. H. Hng, and Q. Y. Yan, *J. Phys. Chem. C.* 115 (2011) 8400.
29. J. X. Zhu, T. Zhu, X. Z. Zhou, Y. Y. Zhang, X. W. Lou, X. D. Chen, H. Zhang, H. H. Hng, and Q. Y. Yan, *Nanoscale* 3 (2011)1084.
30. B. Wang, X. L. Wu, C. Y. Shu, Y. G. Guo, and C. R. Wang, *J. Mater. Chem.* 20 (2010) 10661.
31. Y. J. Mai, X. L. Wang, J. Y. Xiang, Y. Q. Qiao, D. Zhang, C. D. Gu, and J. P. Tu, *Electrochim. Acta.* 56 (2011) 2306.
32. M. D. Stoller, S. Park, Y. W. Zhu, J. H. An, and R. S. Ruoff, *Nano Lett.* 8 (2008) 3498.
33. S. Park, J. H. An, I. W. Jung, R. D. Piner, S. J. An, X. S. Li, A. Velamakanni, and R. S. Ruoff, *Nano Lett.* 9 (2009) 1593.
34. C. Lee, X. D. Wei, J. W. Kysar, and J. Hone, *Science* 321 (2008) 385.
35. W. S. Hummers and R. E. Offeman, *J. Am. Chem. Soc.* 80 (1958) 1339.
36. F. Tuinstra, J. L. Koenig, *J. Chem. Phys.* 53 (1970) 1126.
37. S. Stankovich, D. A. Dikin, R. D. Piner, K. A. Kohlhaas, A. Kleinhammes, Y. Y. Jia, Y. Wu, S. T. Nguyen, R. S. Ruoff, *Carbon* 45 (2007) 1558.
38. S. Park, J. H. An, I. W. Jung, R. D. Piner, S. J. An, X. S. Li, A. Velamakanni, R. S. Ruoff, *Nano Lett.* 9 (2009) 1593.